Effect of Postweld Treatment on the Fatigue Crack Growth Rate of Electron-Beam-Welded AISI 4130 Steel

CHIEN-CHUN WANG and YIH CHANG

This article studies the effect of *in*-chamber electron beam and *ex*-chamber furnace postweld treatments on the fatigue crack growth rate of electron-beam-welded AISI 4130 steel. Mechanical properties of the weldment are evaluated by tensile testing, while the fatigue properties are investigated by a fatigue crack propagation method. Microstructural examination shows that both postweld treatments temper the weldment by the appropriate control of beam pattern width, input beam energy, and furnace temperature. In addition, the ductility, strength, and microhardness of the weldment also reflect this tempering effect. The fatigue crack growth rate is decreased after both postweld treatments. This is mainly caused by the existence of a toughened microstructure and relief of the residual stress due to the fact that (1) the residual stress becomes more compressive as more beam energy is delivered into the samples and (2) postweld furnace tempering effectively releases the tensile stress into a compressive stress state.

I. INTRODUCTION

THE electron beam (EB) is used widely in many applications, such as welding, cutting, annealing, surface modification, lithography, and analyses, and for many types of materials, such as metals, alloys, ceramics, and semiconductors, due to its high efficiency of delivering focused energy into the material under a controlled manner.[1] When applying EB to the welding of metals in vacuum, the inherent advantages of the weldment include high aspect ratio, low contamination, deep penetration, and a narrow heat-affected zone (HAZ).[2,3,4] Therefore, the mechanical properties of EB-welded parts are comparable to those of base metal since the EB welding induced defects and deformation resulting from the microstructure transformation, and inhomogeneous temperature gradient can be limited to a very narrow region.[4,5]

However, when the EB-welded specimens are subjected to a fatigue loading, the position of failure or fracture is always in the hard and brittle fusion zone or near the HAZ due to defects such as undercut, lack of penetration, and microvoids existing in these regions.[6,7] In this case, most of the fatigue life is consumed in the fatigue crack propagation period.[8] Therefore, residual stress, ever present in the surface and interior of the EB-welded joints, has a marked influence on the fatigue crack growth behaviors. It is reported that the residual stress of the EB-welded steel plate perpendicular to the fusion zone both in the surface and interior is compressive in the plate thickness direction using a slicing method to measure the three-dimensional residual stress distribution.[5] In contrast, using a step-by-step drilling method,[9] the surface residual stress of the fusion zone has been determined to be tensile while that of the interior is compressive. Fukuda and Tsuruta[10] have investigated the residual stress effect on the fatigue behaviors and point out that the residual stress is redistributed during the fatigue crack growth process, and at the same time, the compressive residual stress is gradually reduced to nearly zero. In our early study of EB welding,[9] the resistance to the near-threshold fatigue crack growth was shown to be improved by the reduction of the tensile residual stress on the surface. It is also known that the tensile residual stresses increase the fatigue crack propagation rate, da/dN,[11] whereas the compressive stress can retard the early stage of crack growth and the more compressive the stress, the more obvious the retarding effect will be.[12] Therefore, the stress-relief treatment can significantly redistribute the residual stress and change the fatigue behaviors of the weldment.

With a view to improving the hard and brittle weld structure, fatigue properties, and fracture toughness of the weldment, the postweld heat treatment should be considered to obtain toughened microstructures and to relieve the residual stress of the weldment. In addition, in-chamber EB tempering with a lower energy input in the vacuum chamber immediately after the EB welding provides the further advantages of time saving (no pumping time) and high quality (vacuum treatment). In this study, two postweld treatments, *in*-chamber EB postweld heat treatment (EBPWHT) and *ex*-chamber furnace postweld heat treatment (FPWHT), are employed to temper the weldment and release the residual stress to improve the fatigue properties of the EB-welded AISI 4130 steel.

II. EXPERIMENTAL PROCEDURES

A commercial AISI 4130 alloy steel with the specimen dimensions 200 × 50 × 3 mm is used for the present study. Table I lists the nominal chemical composition of this material. After quenching and tempering treatment at 490 °C for 3 hours, specimens with a Rockwell hardness of H_{Rc} 33 to 37 are welded using a Sciaky (Chicago, Ill., USA) high-vacuum-type EB machine with a maximum power capacity of 30 kW. The beam parameters of accelerating voltage, beam

CHIEN-CHUN WANG, formerly Lecturer, Department of Mechanical Engineering, Chung Cheng Institute of Technology, is Ph.D. Candidate, Institute of Mechanical Engineering, National Taiwan University, Taipei, Taiwan, 106, Republic of China YIH CHANG, Associate Professor, is with the Department of Mechanical Engineering, Chung Cheng Institute of Technology, Tao-yuan, Taiwan 335, Republic of China.

Manuscript submitted November 7, 1995.

Table I. Nominal Composition of AISI 4130 Steel

Element	C	Si	Mn	Cr	Mo	Ni	Cu	Fe
Wt pct	0.33	0.29	0.53	0.90	0.21	0.03	0.03	bal

current, and heat input are selected large enough to obtain full penetration in each weld and are, respectively, 50 kV, 70 mA, and 103 J/mm for 3-mm-thick steel samples. After EB welding, two postweld heat treatments are adopted. One is the EBPWHT in the vacuum chamber performed immediately after the welding. In order to obtain a uniform distribution of temperature and avoid surface remelting during EB tempering, a computer-control-generated microdot pattern, as shown in Figure 1, developed by the Sciaky company, is employed to raster the specimen by varying the pattern width, beam energy, and scan speed. The other is the FPWHT by taking the specimen out of the vacuum chamber and putting it into the conventional heating furnace under different tempering temperatures. Table II summarizes the processing conditions for these two postweld heat treatments.

The step-by-step hole-drilling method[13,14] is used to evaluate the influence of residual stress on the fatigue properties of postweld 4130 alloy steel. Since the drilled hole is a 1.0 mm in diameter and 1.2 mm in total depth with a 0.1-mm interval as specified by ASTM E387-85,[14] it is important to recognize that the measured and calculated residual stress, based on the readings from the strain gage pasted near the fusion zone, represents the average stress level between the indicated hole depth and the top surface, where the stress level is zero under the assumption of the plane stress. Welded specimens are also inspected to check if there are any weld porosities in the fusion zone using the X-ray transmission method. These porosities are generated as the EB focuses onto and reacts with the sample to induce the temperature of the melt pool sufficiently high enough to cause the base metal and/or low-melting-point elements to become vapor, which is then trapped during rapid solidification. However, no porosity is resolved since the thickness of the specimen is thin enough to allow any gas bubbles to reach the free surface. The microstructure of the welded zone is examined by an optical microscope and the fracture surface is investigated by a scanning electron microscope (SEM).

The simple tensile and fatigue crack propagation tests are all performed on a computerized MTS closed-loop servohydraulic testing machine, where the orientation of the welded specimens to show the locations of the fusion zone, HAZ, and crack is schematically shown in Figure 2. As shown in Figure 2(a), the configuration of a tensile test specimen with the fusion zone in the middle of the gage length accords with the ASTM E8M-89 specification.[15] Compact tension (CT) specimens machined from the welded samples are used to measure the fatigue crack growth rate, da/dN, where a is the crack length and N is the fatigue life cycle. The experimental method and the specimen configuration follow the instructions of ASTM E647-88a,[16] in which the precrack and crack grow along the weld, as shown in Figure 2(b). A sinusoidal load with frequency 40 Hz and stress ratio $R = 0.1$ is applied throughout this study. A clip-on gage is attached to the front face of the CT specimen to measure the crack-opening displacement on which the growing fatigue crack length can be determined. The fatigue cycles and the cyclic stress intensity at every moment of stress can be automatically indicated on a printer which is connected to the computer. Therefore, the curves of fatigue crack growth rate are plotted based on the Paris equation:[17]

$$da/dN = C(\Delta K)^n$$

where da/dN is the fatigue crack growth rate, C is a pro-

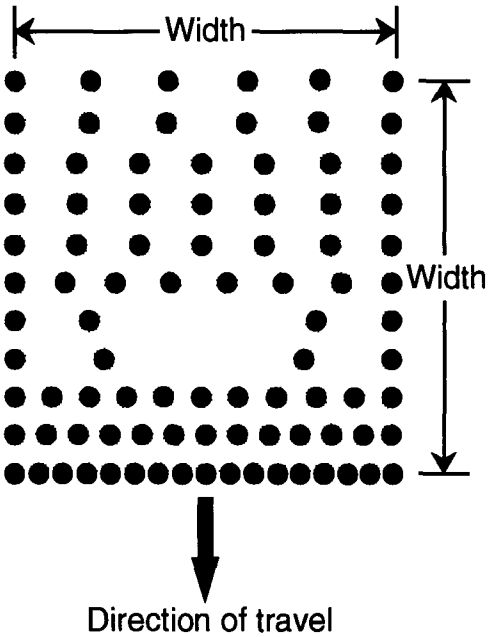

Fig. 1—The microdot pattern of electron beam used in the postweld EB tempering where the width is a controlled processing parameter.

Table II. Processing Parameters of EB and Furnace Postweld Treatment

Specimen	Microdot Pattern Width (mm)	Power (W)	Voltage (kV)	Current (mA)	Velocity (mm/min)	Heat Input (J/mm)
EB1	3	720	45	16	635	68
EB2	6	720	45	16	635	68
EB3	6	225	45	5	254	53
EB4	9	720	45	16	635	68
F1	550 °C furnace tempering temperature for 1 h and air cooling					
F2	480 °C furnace tempering temperature for 1 h and air cooling					
F3	400 °C furnace tempering temperature for 1 h and air cooling					
F4	320 °C furnace tempering temperature for 1 h and air cooling					
AW	no tempering treatment and used as reference sample					

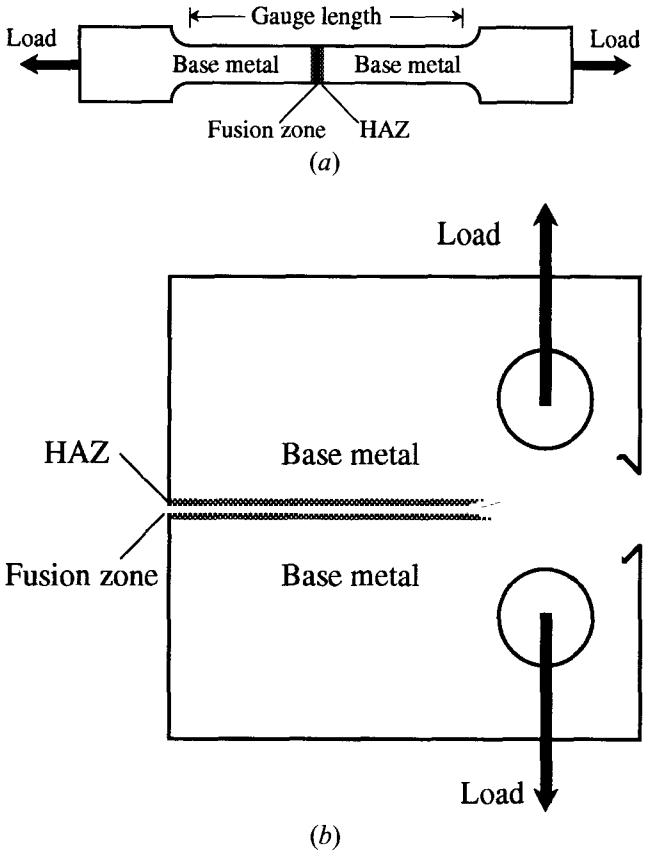

Fig. 2—Schematic diagrams to show the locations of the fusion zone, HAZ, and crack for (*a*) tensile and (*b*) CT (fatigue) specimens.

portional constant, ΔK is the stress intensity factor, and n is a constant.

III. RESULTS AND DISCUSSIONS

Figure 3 shows typical microstructures of the cross section of HAZ and base metal after EB welding but before postweld treatment. The base metal is basically a tempered martensite, whereas the main constituents in the HAZ are mixtures of fine-grained and coarse-quenched martensites. Figure 4 shows the representative micrographs of the fusion zone under as-welded and different postweld heat treatments. As shown in Figure 4(a), the microstructure of the as-welded specimen is a typical quenched martensite. The EBPWHT, as shown in Figure 4(b) is a mixture of quenched martensite and partially tempered martensite, whereas the FPWHT, as shown in Figure 4(c), is full of tempered martensite. Therefore, both postweld heating processes (EBPWHT and FPWHT) do temper the microstructure of the weldment to become tempered martensite.

Table III lists the tensile properties of as-welded and heat-treated specimens. For the EBPWHT specimens irradiated with the same microdot-pattern width of 6 mm (comparing samples EB2 and EB3 to AW), the strength decreases less with a lower heat input. This is also consistent with the microhardness profiles, as shown in Figure 5(a), where the overall microhardness in the central fusion zone decreases less with a lower EB energy input. This is because the lower heat input implants less EB energy into

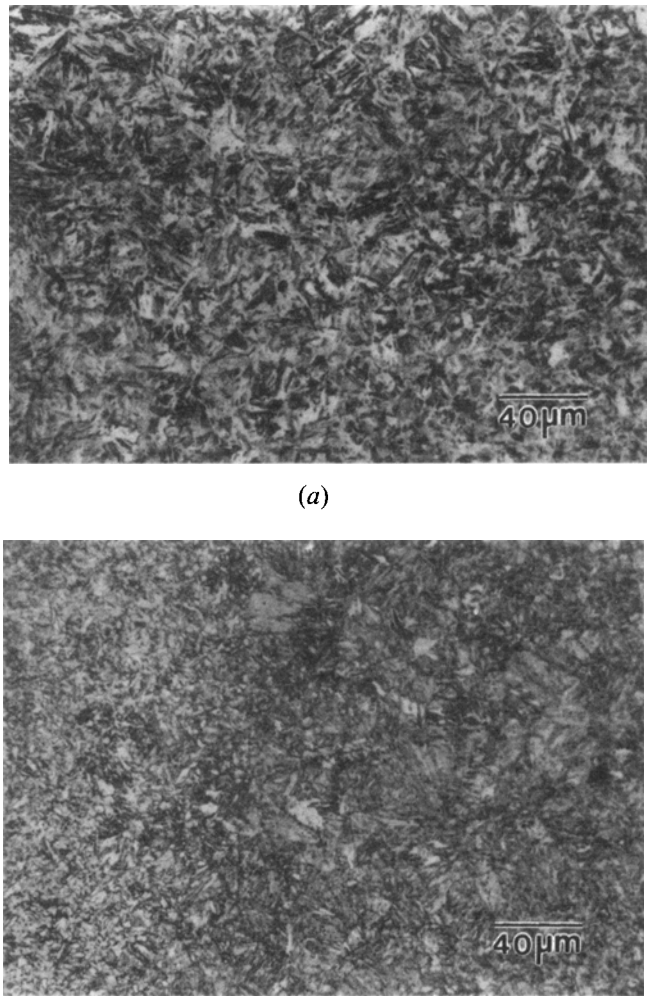

Fig. 3—Microstructures of the cross section of (*a*) HAZ and (*b*) base metal after EB welding but before postweld treatment. Base metal is basically the tempered martensite and HAZ is a mixture of fine-grained and coarse-quenched martensite.

the sample and results in less softening. For the EBPWHT specimens delivered with the same heat input 68 J/mm (samples EB1, EB2, and EB4 in Table III), the strength increases with the increase of pattern widths from 3 to 9 mm. This can be further confirmed with the microhardness profile, as shown in Figure 5(b), where the microhardness in the central fusion zone decreases more with the decrease of pattern width. The same heat input with more narrow pattern width delivers the same heat into a smaller area and, therefore, induces a higher temperature to temper the quenched martensite in the central fusion zone. This phenomenon is similar to that of the FPWHT specimens, as shown in Figure 6, where higher postweld furnace temperatures transform more quenched martensite into tempered martensite with a lower hardness in the central fusion zone. Since the 400 °C furnace temperature significantly reduces the microhardness from Hv 490 to 390 on average, as shown in Figure 6, the tempering effect of the EB postweld treatment with the highest heat input (68 J/mm) and narrowest 3-mm-pattern width employed in this study is not as effective as that of the FPWHT specimen furnace tempered at 400 °C. The microstructure shown in Figure 4 also

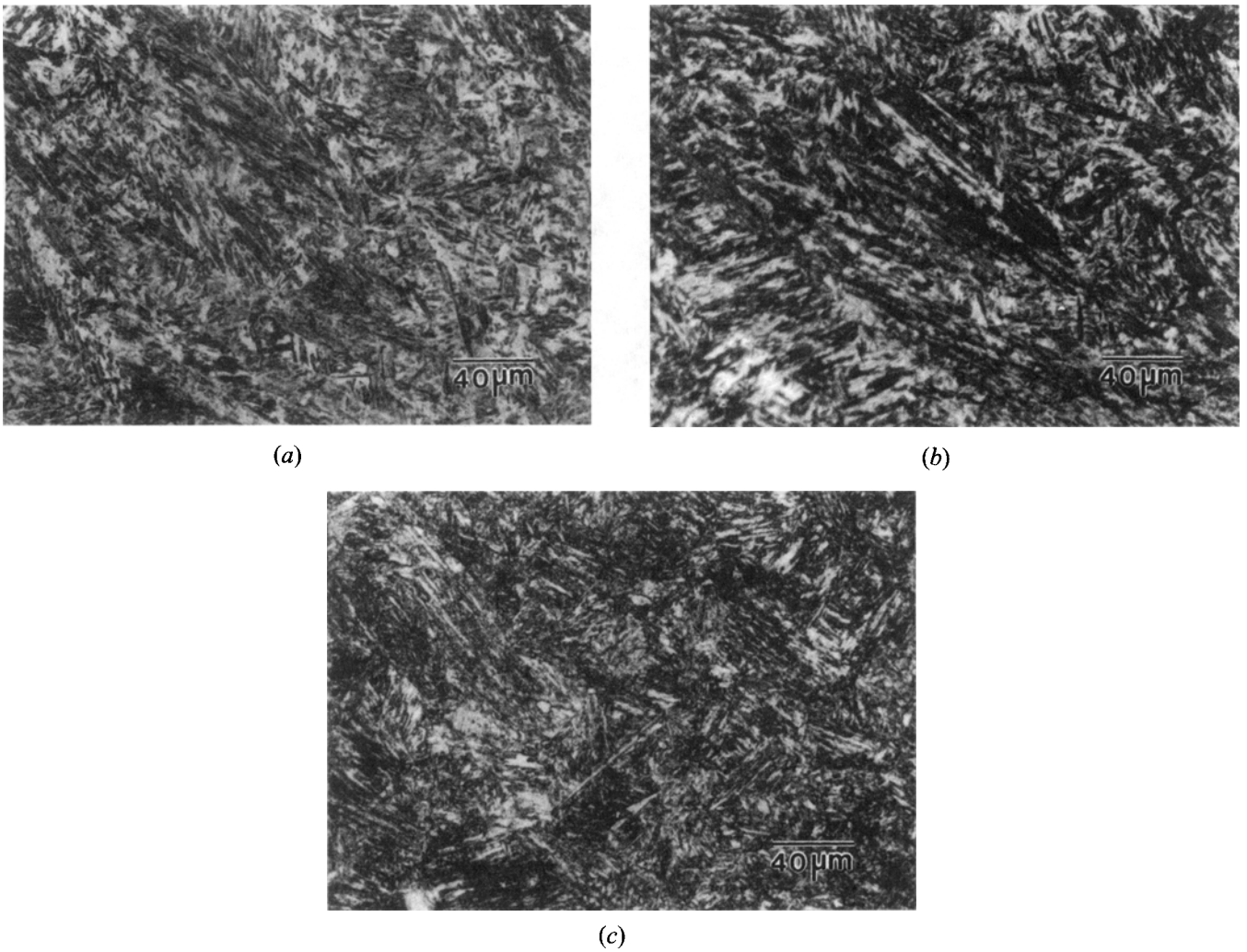

(*a*) (*b*) (*c*)

Fig. 4—Microstructures of fusion zone after (*a*) as-welded (sample AW), (*b*) EBPWHT (sample EB1), and (*c*) FPWHT (sample F1). The as-welded specimen mainly contains quenched martensite. The EBPWHT is a mixture of quenched martensite and partial tempered martensite, whereas the FPWHT is full of tempered martensite.

Table III. Mechanical Properties of EBPWHT and FPWHT Specimens

Specimen	Ultimate Strength (MPa)	Yield Strength (MPa)*	Elongation (Pct)	Reduction of Area (Pct)	Position of Failure
EB1	1010	980	7.4	43	base metal
EB2	1090	1080	5.5	40	base metal
EB3	1120	1099	5.2	34	base metal
EB4	1148	1199	6	36	base metal
F1	1001	970	8.2	44	HAZ
F2	1110	1080	6.3	40	base metal
F3	1199	1100	6.4	37	base metal
F4	1138	1128	7.1	35	base metal
AW	1140	1120	5.5	33	base metal

*0.2 pct offset.

accounts for this behavior since the EBPWHT specimen only has a partially tempered structure but the FPWHT sample is fully tempered martensite.

The depth profiles of the residual stress of EBPWHT and FPWHT specimens in the fusion zone are shown in Figures 7 and 8, respectively. As shown in Figure 7(a), the residual stress of the as-welded sample (AW specimen) above 0.3 mm is in a tensile stress state, whereas below that a compressive stress state is developed. Furthermore, the residual stress becomes more compressive as the depth increases into the weld. However, after tempering by EB heating, the residual stress becomes more compressive if more energy is delivered into the samples. This is shown in Figure 7(a), where the higher heat input, 68 J/mm, has a more pro-

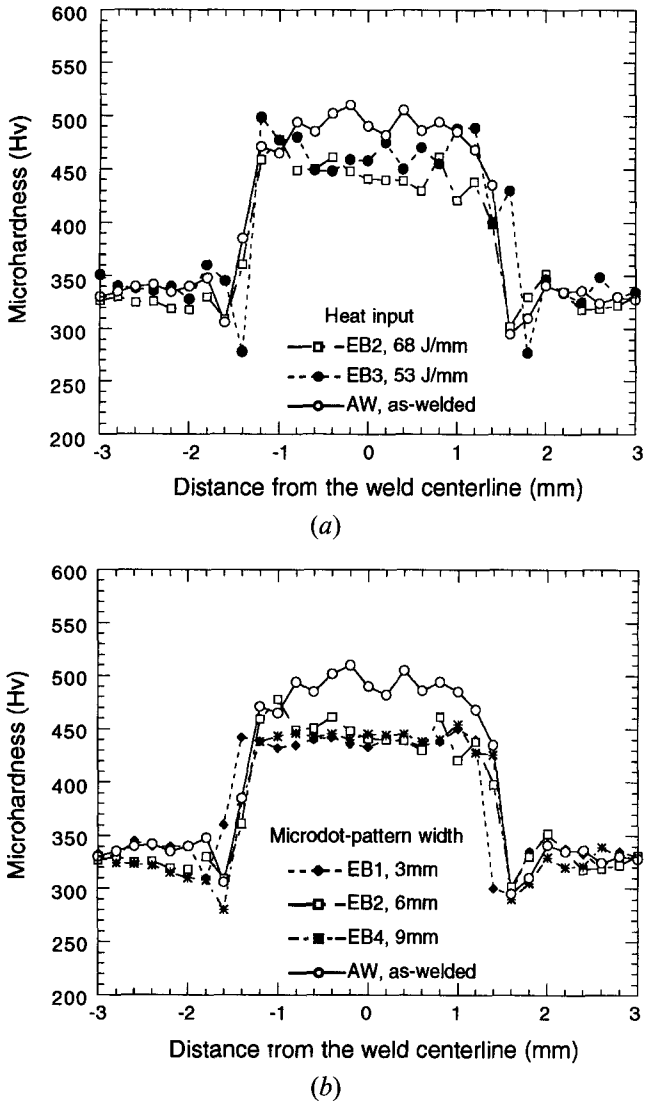

Fig. 5—Microhardness profiles of EBPWHT specimens: (*a*) same microdot-pattern width of 6 mm with different heat input and (*b*) same heat input of 68 J/mm with different microdot-pattern width.

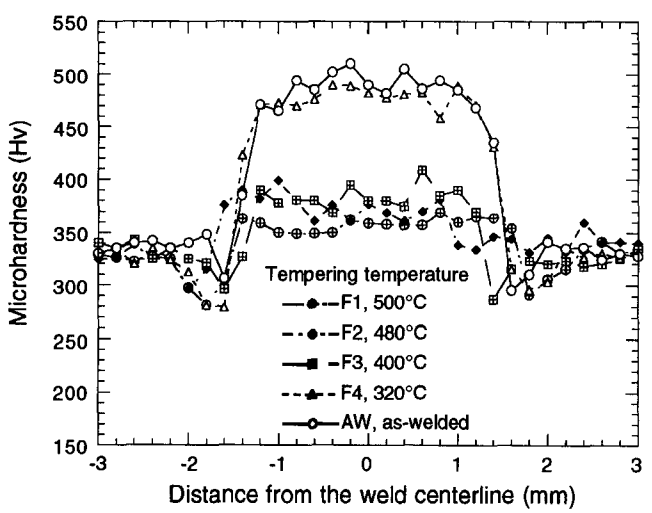

Fig. 6—Microhardness profiles of as-welded and FPWHT specimens with tempering temperatures at 320 °C, 400 °C, and 500 °C.

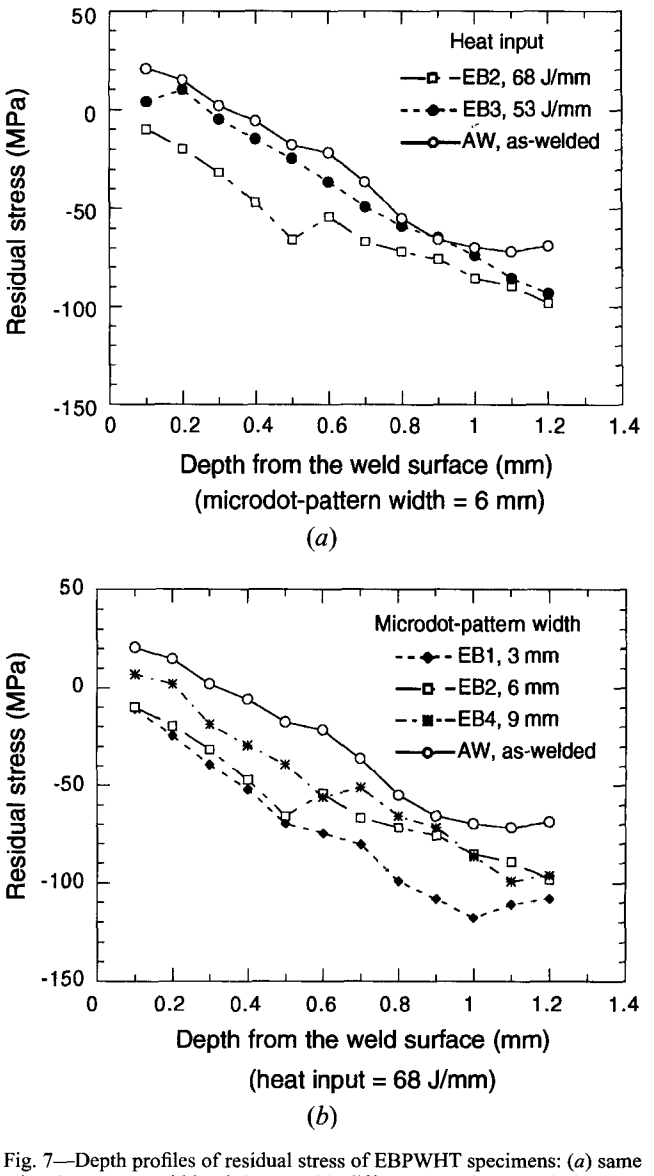

Fig. 7—Depth profiles of residual stress of EBPWHT specimens: (*a*) same microdot-pattern width of 6 mm with different heat input and (*b*) same heat input of 68 J/mm with different microdot-pattern width.

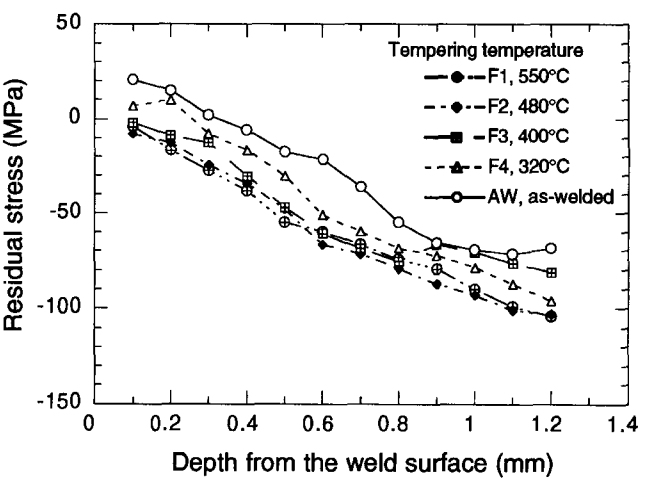

Fig. 8—Depth profiles of residual stress of FPWHT specimens.

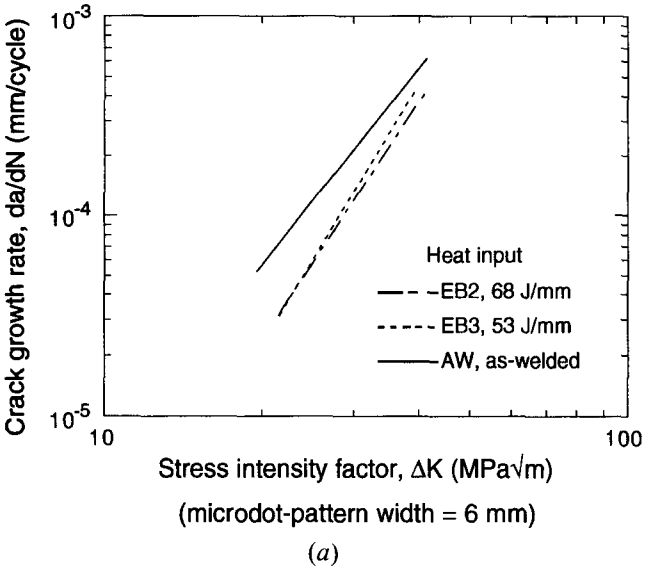

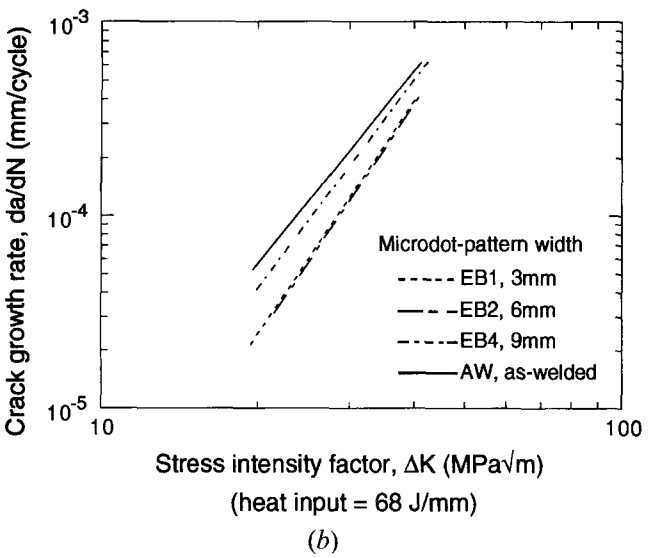

Fig. 9—Effect of EBPWHT on fatigue crack growth rate: (*a*) same microdot-pattern width of 6 mm with different heat input and (*b*) same heat input of 68 J/mm with different microdot-pattern width.

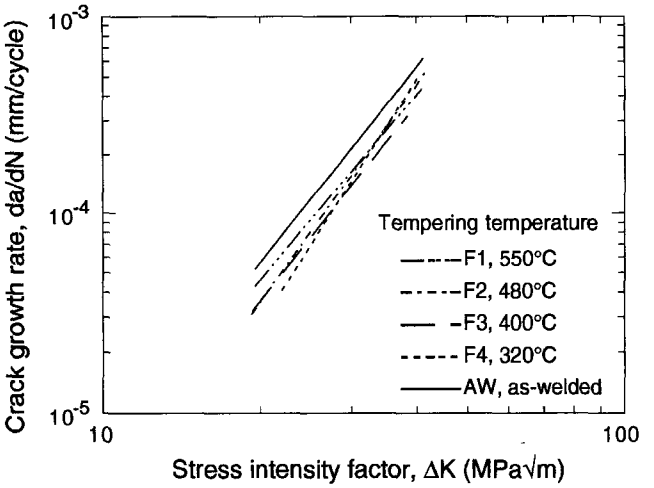

Fig. 10—Effect of tempering temperature of FPWHT specimens on fatigue crack growth rate.

Table IV. Fatigue Crack Growth Data: Curve-Fitted *C* and *n* Values in the Paris Equation

Specimen	*n*	*C*
EB1	3.75	3.75×10^{-11}
EB2	3.57	1.18×10^{-10}
EB3	3.93	1.68×10^{-11}
EB4	2.92	6.31×10^{-9}
F1	2.73	1.74×10^{-8}
F2	3.14	1.79×10^{-9}
F3	2.26	1.35×10^{-7}
F4	3.56	1.62×10^{-10}
AW	3.16	2.26×10^{-9}

nounced compressive residual stress state than that of the lower heat input, 53 J/mm. Besides, as shown in Figure 7(b), the residual stress becomes more compressive by narrowing the microdot-pattern widths from 9 to 3 mm. Not only for EBPWHT but for FPWHT samples, as shown in Figure 8, do the higher postweld furnace tempering temperatures effectively release the tensile stress into a compressive stress state.

For the fatigue crack propagation test, the fatigue cracks grow along the fusion zone, which is parallel to the weld direction. The curves of fatigue crack growth rate can be reconstructed by curve fitting to the Paris equation using the least square method and replotted in Figures 9 and 10 for EBPWHT and FPWHT specimens with *C* and *n* values listed in Table IV. Figure 9(a) shows the effect of heat input and Figure 9(b) shows the effect of microdot-pattern width of EBPWHT specimens on the fatigue crack growth rate. As shown in Figure 9(a), the EBPWHT specimen with larger heat input has better resistance to fatigue crack propagation. In addition, as shown in Figure 9(b), the narrower pattern width has slower fatigue crack growth rate for the same heat input, 68 J/mm, whereas if the pattern width is smaller than 6 mm, the fatigue crack growth rate is almost the same. Figure 10 shows the effect of tempering temperature on the fatigue crack growth rate. It is found that tempering temperatures above 320 °C are enough to cause the reduction of crack growth rate. Furthermore, by comparing Figure 9 with Figure 10, the postweld treatments, both EBPWHT and FPWHT, can be used to improve the resistance to fatigue crack growth. Since the residual stress state is believed to be a dominant factor to affect the fatigue behaviors of the weldment,[9-12,18,19] by comparing Figures 9 and 10 with Figures 7 and 8, it can be found that compressive residual stress indeed retards the fatigue crack growth rate.

Table III also shows that the position of failure in the tensile test of as-welded and both postweld treatments is in the base metal, except the F1 specimen is in the HAZ. Since the 500 °C postweld tempering treatment of the F1 specimen in furnace for 1 hour is higher than that of the base material, which is 490 °C for 3 hours before EB weld, we believe the position of failure may extend from the base metal into the HAZ. The fact that the position of failure of all other specimens is in the base metal indicates that the strength of weldment is higher than that of base metal and HAZ for specimens after postweld treatment.

Figure 11 shows the fatigue fractographs for the as-welded, EBPWHT, and FPWHT specimens all with a stress intensity factor ΔK of 22 MPa$\sqrt{m}$. As shown in

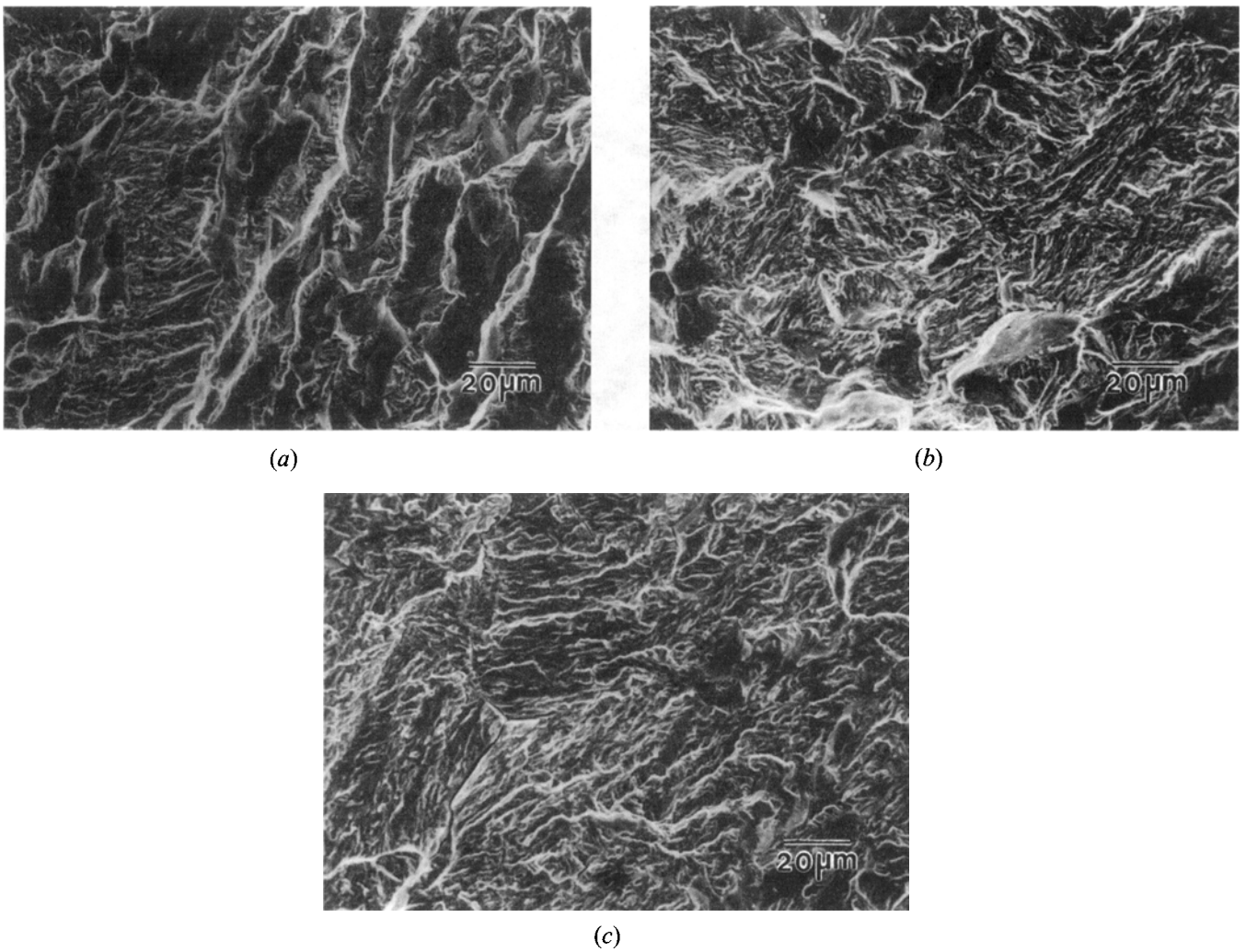

(*a*) (*b*) (*c*)

Fig. 11—Fatigue fractographs at $\Delta K = 22$ MPa$\sqrt{\text{m}}$ for (*a*) as-welded, (*b*) EBPWHT, and (*c*) FPWHT specimens.

Figure 11(a), a large portion of the fracture surface of as-welded specimen is basically an intergranular fracture with fatigue crack branch visible on the surface. The typical fracture surface of EBPWHT specimens, as shown in Figure 11(b), is a mixed mode of intergranular and transgranular fracture, whereas the fatigue fracture mode of FPWHT specimen, as shown in Figure 11(c), is almost a transgranular and ductile fracture. This phenomenon indicates that FPWHT specimens have better ductility than EBPWHT specimens. This is also consistent with the microstructure shown in Figure 4 and the mechanical properties shown in Table III, where the elongation and reduction of area of FPWHT specimens in average are slightly larger than those of EBPWHT specimens.

IV. SUMMARY

In summary, both EB and furnace postweld heat treatments temper the centerline weld microstructure to become tempered martensite. Therefore, strength is decreased but ductility is increased, and microhardness in the central area is lowered. Postweld heat treatments with both EB and furnace tempering indeed improve the resistance to fatigue crack growth. This results from the tempering effect to produce the tempered martensite and the change of residual stress state from initial tensile to final more compressive stress.

REFERENCES

1. S. Schiller, U. Hisig, and S. Panzer: *Electron Beam Technology*, John Wiley and Sons, Inc., New York, NY, 1982.
2. J. Powers: *Weld J.*, Res. Suppl., 1984, vol. 63, p. 39.
3. G.L. Mara, E R. Funk, R.C. Mcmaster, and P.E. Pence: *Weld. J.*, Res. Suppl., 1974, vol. 39, p. 246s.
4. I.G. Prıce: *Met. Constr.*, 1981, vol. 13, p. 612.
5. Y. Ueda, Y.C. Kim, and A. Umekuni: *Trans. JWRI*, 1986, vol. 15 (1), p. 125.
6. Y. Arata, M. Tomie, M. Abe, and E. Abe: *Trans. JWRI*, 1986, vol. 15, p. 35.
7. K. Horikawa, A. Sakakibara, and T. Mori: *Trans. JWRI*, 1983, vol. 12 (2), p. 135
8. L.P. Pook and N.N. Frost· *Int. J. Fract.*, 1973, vol. 9 (1), p. 53.
9. J.R. Hwang and H.H. Chang: *Eng. Fract. Mech.*, 1993, vol. 45 (4), p. 519.
10. S. Fukuda and Y. Tsuruta: *Trans. JWRI*, 1978, vol. 7, p. 67.
11. S. Fukuda, S. Watari, and K. Horıkawa: *Trans. JWRI*, 1979, vol. 8, p. 105.
12. J.L. Doong, T.J. Chen, and Y.H. Tan: *Eng. Fract. Mech.*, 1989, vol. 33, p. 483.

13. *Measurement of Residual Stressed by the Hole-Drilling Strain-Gage Method*, Technical Note TN-503-2, Measurements Group, Inc., Raleigh, NC, 1986.
14. ASTM Specification E 837-89, ASTM, Philadelphia, PA, 1989, vol. 03.01, p. 713.
15. ASTM Specification E 8M-89, ASTM, Philadelphia, PA, 1989, vol. 03.01, p. 147.
16. ASTM Specification E 647-88a, ASTM, Philadelphia, PA, 1989, vol. 03.01, p. 646.
17. P.C. Paris and F. Erdogan: *J. Basic Eng.*, 1963, vol. 85 (4), p. 528.
18. K. Horikawa and Y. Takada: *Trans. JWRI*, 1984, vol. 13 (1), p. 163.
19. C. Kim, D.E. Diesburg, and G.T. Eldis: *Effect of Residual Stress on Fatigue Fracture of Case Hardened Steels*, ASTM STP 776, ASTM, Philadelphia, PA, 1982, p. 224.